Journal of the Mechanical Behavior of Biomedical Materials 78 (2018) 56–64

Contents lists available at ScienceDirect

Journal of the Mechanical Behavior of Biomedical Materials

journal homepage: www.elsevier.com/locate/jmbbm

Contributions of the layer topology and mineral content to the elastic modulus and strength of fish scales

Sandra Murcia[a], Yuri Miyamoto[a], Megha Pratap Varma[a], Alexander Ossa[b], Dwayne Arola[a,c,*]

[a] Department of Materials Science and Engineering, University of Washington, Seattle, WA, USA
[b] Production Engineering Department, School of Engineering, Universidad Eafit, Medellín, Colombia
[c] Department of Mechanical Engineering, University of Washington, Seattle, WA, USA

ARTICLE INFO

Keywords:
Apatite
Collagen
Elastic properties
Fish scales
Rule of mixtures

ABSTRACT

Fish scales are an interesting natural structural material and their functionality requires both flexibility and toughness. Our previous studies identified that there are spatial variations in the elastic properties of fish scales corresponding to the anatomical regions, and that they appear to be attributed to changes in the microstructure. In the present study, a model is proposed that describes the elastic behavior of elasmoid fish scales in terms of the relative contributions of the limiting layer and both the internal and external elasmodine. The mechanical properties of scales from the *Megalops atlanticus* (i.e. tarpon) were characterized in tension and compared with predictions from the model. The average error between the predicted and the experimental properties was 7%. It was found that the gradient in mineral content and aspect ratio of the apatite crystals in the limiting layer played the most important roles on the elastic modulus of the scales. Furthermore, misalignment of plies in the external elasmodine from the longitudinal direction was shown to reduce the elastic modulus significantly. This is one approach for modulating the fish scale flexibility for a high mineral content that is required to increase the resistance to puncture.

1. Introduction

Over the past decade, natural dermal armors have served as a source of inspiration for the design of new engineering materials (Li et al., 2012; Chintapalli et al., 2014; Funk et al., 2015; Martini and Barthelat, 2016). Among the wide range of dermal armors being explored (Yang et al., 2013), several studies have focused on elasmoid fish scales (Lin et al., 2011; Garrano et al., 2012; Zhu et al., 2012; Yang et al., 2013; Gil-Duran et al., 2016), which are unique from the more rigid cosmoid, ganoid and placoid scales (Sherman et al., 2016). Elasmoid scales are much thinner and stacked or over-layered with respect to one another. They are characteristic of fish with greater speed, and could be considered multi-functional as their flexibility is arguably just as important as their resistance to puncture (Bruet et al., 2008; Jandt, 2008). Flexibility in these dermal armors is achieved by their construction, and apparently from the stacking sequence of the principal layers.

The overall structure of elasmoid scales consists of three distinct layers across its thickness (Fig. 1A). The Limiting layer (LL) is the most highly mineralized region of the scale. It serves as the outermost coating of the scales and as such is regarded as the first barrier against penetration (Zhu et al., 2012). The elasmodine is a laminate consisting of discrete plies of unidirectionally aligned collagen fibers with a diameter of between 100 and 160 nm (Zylberberg and Nicolas, 1982; Garrano et al., 2012). The individual plies of the elasmodine are rotated at specific angles with respect to one another and exhibit a unique thickness, which depends on the fish (Murcia et al., 2016a). Based on earlier reports (Zylberberg and Nicolas, 1982; Zylerberg, 1985; Sire and Huysseune, 2003), the mineralization front extends from the LL into the underlying collagen matrix of the elasmodine. According to the distribution in mineral content, the elasmodine is further divided into external (EE) and internal (IE) regions, with the EE possessing the larger mineral content of the two.

Previous studies on the mechanical behavior of fish scales have revealed that the strength and elastic modulus of the scales are largely dependent on the number of mineralized plies of the EE, and the ratio of the elasmodine thickness to the total scale thickness (i.e. elasmodine ratio) (Murcia et al., 2015, 2016b). The rule of mixtures is commonly adopted as a first approach to describe the elastic behavior of composite materials based on the contributions of the constituents. Although a model for the elastic properties of scales has been presented (Zhu et al., 2012), it was not based on an explicit description of the contributions from the LL, EE and IE of the scales. Owing to the differences in mineral

* Correspondence to: Department of Materials Science and Engineering, University of Washington, Roberts Hall, Box 352120, Seattle, Washington 98195, USA.
E-mail address: darola@uw.edu (D. Arola).

https://doi.org/10.1016/j.jmbbm.2017.11.010
Received 16 August 2017; Received in revised form 29 October 2017; Accepted 6 November 2017
Available online 07 November 2017

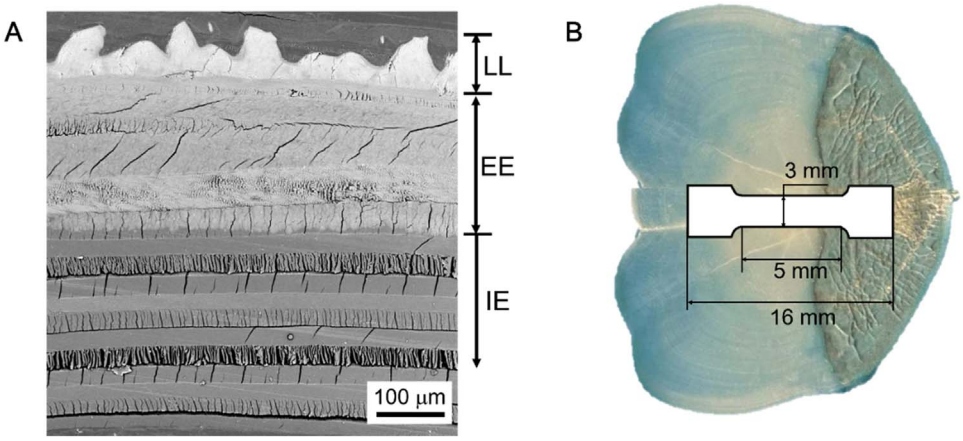

Fig. 1. Details of the evaluation involving tensile testing of the scales. A) cross-section of a representative tarpon scale denoting the three distinct regions including the limiting layer (LL), external elasmodine (EE) and internal elasmodine (IE). B) Location and geometry of a stamped tensile specimen from a representative tarpon scale.

content of these three layers and their distribution, these factors should be considered in descriptions of the elastic behavior. Furthermore, the lamina orientations in the elasmodine is not the same for all fish (Murcia et al., 2016a) and is potentially an important contributor to the elastic properties as well.

Earlier studies concerning the contribution of the individual layers of scales to the mechanical properties have evaluated the strength and elastic modulus of the IE and mineralized layers separately. A summary of the tensile properties from these investigations is listed in Table 1. The elastic modulus of the mineralized layers is significantly larger than that of the whole scale, which apparently results from the large mineral gradient. Whereas properties of the IE are largely controlled by the stretching of unidirectional collagen fibrils, the properties of the EE and LL have not been reported individually due to the difficulty in achieving separation. For the *M. saxatilis,* the properties of the mineralized layers were estimated using the rule of mixtures assuming the volume fraction of the IE is equal to the sum of the volume fractions of the EE and LL. However, it is not clear that this ratio is constant over the length of the fish.

Understanding the relative contributions of the mineralized layers and IE to the mechanical behavior of fish scales is necessary to distinguish the principles that guide the scale development and its ability to achieve its multifunctional performance. According to the results of previous studies, the tensile properties and Mode III tear resistance of elasmoid scales are highly correlated with the EE ratio (Murcia et al., 2015, 2016b). However, a detailed analysis of the importance of spatial variations in the scale microstructure on mechanical behavior was not conducted. To the authors' knowledge, no study has developed a microstructure-based model that quantitatively details contributions of the microstructural characteristics to the tensile properties of scales. Therefore, the objective of this study is to develop new knowledge regarding the contributions of the layer topology and the layer composition to the elastic modulus and strength of elasmoid fish scales.

2. Materials and methods

2.1. Experimental approach

Scales from a wild captured *Megalops atlanticus* (i.e. tarpon) were extracted from the body of a single tarpon within three characteristic regions including adjacent to the head, mid-length and near the tail, following established procedures (Murcia et al., 2016a). After extraction the scales were stored in Hanks Balanced Salt Solution (HBSS) at 4 °C and evaluated within a week of harvesting the fish. Conventional dog-bone shaped tensile specimens were sectioned from the scales using a punch and stamping process (Zhang et al., 2007). In recognition of the variation in thickness of the scales (Zhu et al., 2013), a single sample was stamped from the center of each scale where the thickness is most uniform. The specimens possessed a gage section length and width of approximately 5 mm and 3 mm, respectively (Fig. 1). The thickness was measured over the length of the gage section to assess the variation, and in general varied by less than 50 μm over the gage section length. The lowest value was used in calculating stress. In recognition that the scales may exhibit anisotropy due to the different alignment of the collagen fibers (Zhu et al., 2012; Yang et al., 2014; Murcia et al., 2015, 2016a), all of the specimens were obtained with alignment parallel to the fish length.

After sectioning, the specimens were maintained in an HBSS bath at room temperature. Subsequently, the remaining area of the scales outside of the stamped tensile specimen was used for microstructural analysis. A fixation process was adopted that started with submersion in 2% glutaraldehyde buffered with 0.1 M sodium cacodylate with pH = 7.2 for 4 h. They were then rinsed in 0.1 M sodium cacodylate buffer followed by post-fixation in 1% osmium tetroxide buffered with 0.1 M sodium cacodylate for 2 h. After rinsing, the scales were dehydrated through an ascending ethanol series from 50% to 95%, followed by 100% acetone and instant dehydration in 2,2- dimethoxypropane (DMP) for 5 h, and then followed by infiltration of the scales in Mollenhauer resin. The microstructure and fiber orientation of individual lamina were analyzed following established procedures

Table 1
Elastic modulus (E) and strength (S) of scales reported for the *Arapaima gigas* (arapaima), *Megalops atlanticus* (tarpon) *and Morone saxatilis* (striped bass) in the longitudinal direction. The properties are defined in terms of the whole scale thickness, as well as the contribution of the individual layers where available. For the striped bass, the mineralized layer properties were estimated using the rule of mixtures assuming the volume fraction of the IE is equal to the sum of the volume fractions of the EE and LL. All quantities are listed in MPa.

	Entire Scale		IE		EE + LL	
Fish	**E**	**S**	**E**	**S**	**E**	**S**
Arapaima gigas (Yang et al., 2014)	860 ± 320	23.6 ± 7.2	470 ± 250	36.9 ± 7.4	–	–
Megalops atlanticus (Gil et al., 2016)	300 ± 59	24.4 ± 7.1	170	40 ± 8	–	–
Morone saxatilis (Zhu et al., 2012)	~ 860 ± 150	~ 30 ± 10	~ 450 ± 150	~ 65 ± 15	~ 1250	~ 45

(Murcia et al., 2016a). The fixed samples were sputtered with Au/Pd and the microstructure within each region of evaluation was examined with a scanning electron microscopy (SEM) in secondary electron imaging mode (JEOL, model JSM- 6010PLUS/LA, Peabody, MA). Final measurements of the distribution of ply thickness and other features were obtained by post-processing of the SEM images using cellSens (Olympus, Tokyo, Japan).

Tensile testing was performed under displacement control loading using a universal testing machine (Instron ElectroPuls E1000, Norwood, MA). The instrument's load cell has a full-scale range of 250 N and precision of 0.01%. A stroke rate of 0.2 mm/min was utilized, which corresponded to a strain rate of roughly 5×10^{-4} 1/s according to the specimen gage length. Five specimens were prepared from each anatomical region (head, middle and tail), which resulted in a total of 15 specimens that were prepared and evaluated. Mechanical properties of the scales were determined from results of the tension tests using the engineering stress-strain definitions. The elastic modulus (E) was determined using the tangent method for strains less than 1% and the strength (S) was defined by the first significant drop in stress.

2.2. Modeling

The elastic response of a fish scale under in-plane uniaxial tension can be treated as a system of springs in parallel. Due to the layered nature of the scales, the resulting stiffness of the composite can be represented by the contributions of the LL, EE and IE. For a material under uniaxial tension, the restoring force per unit cross-section of material is directly proportional to its stiffness (k) as well as the spring displacement (ΔL) according to

$$\frac{F}{A} = k\frac{\Delta L}{L} \tag{1}$$

where F is the total force applied to the material, A is the cross sectional area and L is the initial length. When defined for a material, the proportionality constant k is an intrinsic property of the material. For a material maintained in the elastic region, Hooke's law can be used to describe the relationship between the stress (σ) and strain (ε) according to

$$\sigma = E\varepsilon \tag{2}$$

As can be seen in Eq. (2), the spring stiffness in Eq. (1) is the elastic modulus of the material. In the case of springs in parallel, the total force of the system is equal to the summation of the response of each component. Therefore, for a material system with n springs, the total axial force (F_T) to achieve a deformation of magnitude ΔL is given by

$$F_T = \sum_{i=1}^{n} A_i E_i \frac{\Delta L_i}{L_i} \tag{3}$$

Since the configuration requires equivalent strain of all components of the system, the effective elastic modulus of the material E_T can be obtained by rewriting Eq. (3) for the modulus as

$$E_T = \sum_{i=1}^{n} \frac{A_i}{A_T} E_i \tag{4}$$

where A_i and A_T are the cross-section areas of the individual layer and total, respectively. If all of the components in the system share the same depth, the area fraction can be reduced to a thickness ratio. Then, accounting for the thickness of the three primary layers (Fig. 1A) of the scales, the elastic modulus of the scales (E*) can be described as

$$E^* = \frac{t_{LL}}{t_T} E_{LL} + \frac{t_{EE}}{t_T} E_{EE} + \frac{t_{IE}}{t_T} E_{IE} \tag{5}$$

If the distribution of the three layers is known as well as their elastic moduli, then the effective elastic response of the scale can be estimated according to Eq. (5).

A previous study on the mineral content of fish scales from different teleost fish found that the volume fraction of mineral in tarpon scales decreases from the LL to the IE (Murcia et al., 2017). The mineral content was maximum at the surface of the LL (70%), and then decreased linearly to 17% at the LL/EE interface. The mineral content remained constant within the EE and then decreased abruptly to negligible content within the IE. Thus, the IE can be treated as layers of unidirectional type I collagen without mineral reinforcement. Both the EE and LL, however, consist of type I collagen reinforced by apatite crystals. As such, the elastic modulus of these layers will be dependent on the volumetric fraction of the reinforcement according to (Jones, 1998)

$$E_c = f_r E_r + f_m E_m \tag{6}$$

where f_r and f_m are the volumetric fractions of the reinforcement and the matrix respectively. This form of the rule of mixtures is widely used for the prediction of properties of continuous, unidirectional composites. However, the reinforcement of the LL and EE does not comply with this condition. The elasmodine of teleost fish scales has been characterized as a laminate structure consisting of lamina of unidirectional collagen fibers that undergo a rotation from ply to ply (Zylberberg and Nicolas, 1982; Bigi et al., 2001; Murcia et al., 2016a) In the EE, the minerals are oriented along the axis of the collagen fibrils (Zylberberg and Nicolas, 1982; Zylerberg, 1985; Sire and Huysseune, 2003) Similarly, bone minerals are oriented along the axis of the collagen fibrils creating a preferred direction (longitudinal axis) (McNally et al., 2012; Schwarcz et al., 2014). However, Currey (Currey, 1969) showed that misalignment of the fibrils in bone reduces the elastic modulus due to the corresponding change in the mineral direction. In the case of fish scales, particular plies of the twisted plywood structure undergo rotation and translation under the applied tensile stress. Specifically, plies oriented 15° to 30° from the tensile axis or less undergo rotation and alignment towards the applied force, whereas plies oriented between roughly 60° to 90° align themselves away from the tensile axis (Zimmermann et al., 2013). Consequently, the collagen fiber orientation of lamina in the EE is an important factor to account for in a prediction of the elastic modulus.

The effect of the misalignment between the loading axis and the reinforcement orientation was studied by Nielsen and Chen (1968). The ratio of elastic modulus between the aligned and misaligned unidirectional composite is described by

$$\frac{E_0}{E_\theta} = \cos^4\theta + \frac{E_0}{E_{90}} sin^4\theta + \left(\frac{E_0}{G} - 2\upsilon\right)\cos^2\theta sin^2\theta \tag{7}$$

where E_θ is the elastic modulus of the plies with reinforcement misalignment of θ, and E_0 and E_{90} are the values of E for alignment angles of 0° (i.e. aligned) and 90° (i.e. orthogonal), respectively. The quantities G and υ are the shear modulus of the composite and the major Poisson's ratio, respectively. Using representative values for the parameters in Eq. (7), Currey (1969) showed that E_θ of bone decreases sharply with increasing misalignment, which emphasizes the importance of accounting for misalignment in the prediction of properties of mineralized tissue. Therefore, predictions for the elastic modulus of elasmoid fish scales should account for the ply orientations when considering the EE contributions. The elastic modulus of the EE (E_{EE}) can then be estimated as

$$E_{EE} = \sum_{i=1}^{EEplies} \frac{t_i}{t_T} E_{\theta_i} \tag{8}$$

where the $E_{\theta i}$ is the elastic modulus of the *ith* ply according to its misalignment angle (θ), and t_i is the ply thickness.

To estimate the elastic response of scales according to Eq. (8) it is necessary to have values for the parameters in Eq. (7). Several studies have characterized the elastic modulus of hydrated tendon using X-ray diffraction techniques, with values ranging between 0.15 and 1 GPa (Kato et al., 1989; Pins and Silver, 1995; An et al., 2004). For the present study, the lower limit was used to represent E_0 of hydrated

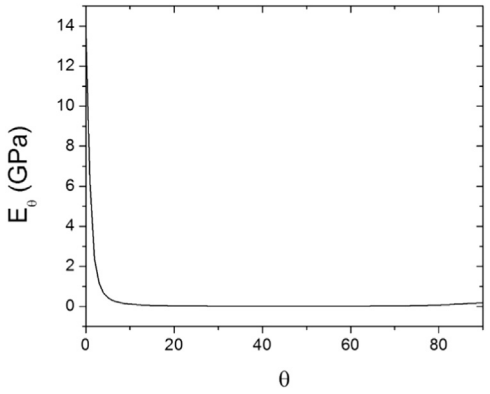

Fig. 2. The effect of crystal misalignment on the elastic modulus of the EE. The orientation θ represents the deviation of the collagen fibers from the longitudinal direction (i.e. tensile axis) in the plies of the elasmodine.

collagen of the IE (E_{IE}). Using an elastic modulus for hydroxyapatite (HA) of 80 GPa (Hench and Wilson, 1993), and volume fraction of mineral of 17%, the E_0 for the EE was estimated to be 13.7 GPa according to Eq. (6). Then, using the inverse rule of mixtures (Jones, 1998), E_{90} for the EE was calculated to be roughly 180 MPa. Similarly, using values for the shear moduli of HA and collagen as 17.3 GPa (Bouslama et al., 2013) and 2.9 MPa (Yang et al., 2008) respectively, the G_{EE} was found to be 3.49 MPa. The effect of collagen fibril orientation on the elastic modulus of plies of the EE is shown in Fig. 2. As evident from this distribution, plies with a misalignment from the longitudinal direction greater than 7° contribute only minimally to the in-plane elastic modulus of the scales.

According to a recent study, mineralization of the LL follows a steep downward gradient from 70% down to 17% at the LL/EE interface (Murcia et al., 2017). Fig. 3 shows an optical image for the LL of a tarpon scale with a discretization scheme used to account for the mineralization gradient. If the gradient in mineral content is known over the unit cell geometry, then the elastic modulus of the LL (E_{LL}) for in-plane tension can be calculated according to

$$E_{LL} = \frac{t_{LL}}{t_T} \sum_{j=1}^{m} \frac{a_j}{a_T} E_j \tag{9}$$

where t_{LL} and t_T are the thickness of the LL and scale, respectively. Here, a_T is the total area of the unit cell and j represent the number of divisions (m) of the cell. Therefore, a_j represents the area of the division j, and E_j is elastic modulus of the slice a_j, which is discussed below. For the tarpon scales the gradient is linear. However, the approach described by Eq. (9) applies for any arbitrary distribution.

A previous evaluation of the LL mineralization revealed that it has a random distribution of mineral crystals (Sire et al., 1997). Therefore, Eq. (6) should not be used in predicting its elastic modulus. Instead, models that account for the shape and distribution of the reinforcement are more appropriate. The Halpin-Tsai equations are often used to predict the properties of mineralized tissues (Nair et al., 2013) but they assume a continuous reinforcement. Nielsen proposed an alternative model for predicting the elastic modulus of random, discontinuous fiber composites (E_{c*}) according to (Nielsen and Chen, 1968; Nielson, 1974)

$$E_{c*} = E_m \left(\frac{1 + A\eta v_r}{1 - \eta\psi v_r} \right) \tag{10}$$

where

$$\psi = 1 + \left(\frac{1 - \phi}{\phi^2} \right) v_r \tag{11}$$

$$A = 2\frac{l}{d} \tag{12}$$

and

$$\eta = \frac{\frac{E_f}{E_m} - 1}{\frac{E_f}{E_m} + A} \tag{13}$$

Here, E_f and E_m are the fiber and matrix moduli, respectively, v_r is the volume fraction of mineral, and l/d is the fiber aspect ratio. Finally, the parameter ϕ is packing fraction or the maximum reinforcement fraction possible while still maintaining a continuous phase, which for random fibers is usually taken as 0.82. The parameter ϕ should not be confused with volume fraction (Lu, 2002). Substituting these quantities enables estimation of the elastic modulus.

3. Results

The microstructural analysis was used to estimate the volume fraction of each layer of the individual scales and results for the middle region are shown in Fig. 4. As evident from the distributions, the IE is the most prevalent component of the tarpon scales, followed by the EE and the LL. These results were fairly consistent across the body of the fish. The overall average volume fraction of these three layers, considering all three anatomic regions, was 0.58 ± 0.07, 0.30 ± 0.05 and 0.12 ± 0.03, respectively. The largest variations in the volume fractions were noted in the EE and LL for scales of the head and middle regions. It is important to highlight that specimen H3 (not shown) and M4 in Fig. 4 exhibited distributions outside of a single standard deviation of the mean response, which could be reflected in the mechanical properties. Scales from the tail exhibited a constant LL volume fraction of about 11%; the largest variation among specimens in this region was in the EE volume fraction. Further information concerning the first ply orientation, number of EE and IE plies, as well as the EE and IE ratios for the scales evaluated are presented in Table 2.

Results of the tensile tests performed on the scales are presented in Fig. 5. Specifically, the elastic modulus and strength of the individual specimens are shown in Fig. 5A and B, respectively. These results are consistent with previous reported values for the elastic modulus and strength of tarpon scales. The maximum elastic modulus was obtained for scales of the head region (~ 350 ± 75 MPa), which was significantly higher than that from the middle and tail regions, and agrees

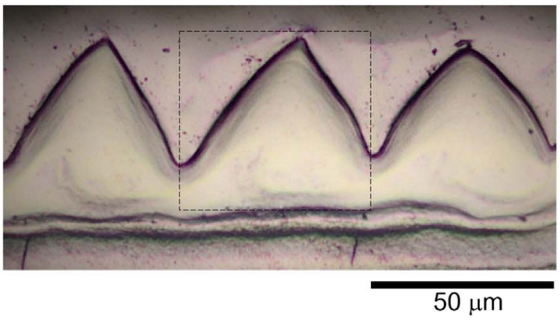

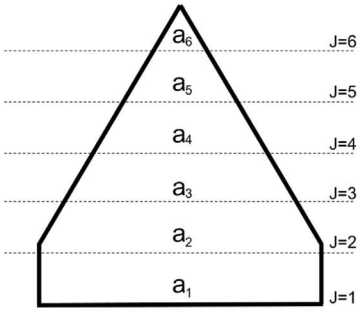

Fig. 3. Geometry of the limiting layer for a representative tarpon scale. As evident from the image (left), the LL has a ridge geometry that repeats over the scale and the ridges can be further discretized into j individual sections (right).

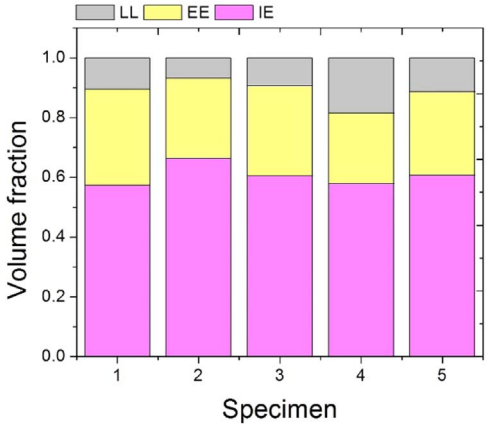

Fig. 4. Distribution of the volume fraction of the limiting layer (LL), external elasmodine (EE) and internal elasmodine (IE) for tarpon scales of the middle region. These specimens are M1, M2, …. to M5. The average volume fraction of these three layers averaged over the head, middle and tail regions was 0.12 ± 0.03, 0.30 ± 0.05, and 0.58 ± 0.07, respectively.

Table 2
Microstructural characteristics of the tarpon scales. The first ply angle was measured CW with respect to the direction of the head of that fish.

Specimen	First ply angle	EE plies	IE plies	Number of plies	EE ratio (%)	IE ratio (%)
H1	163	7	16	23	30	70
H2	140	10	18	28	36	64
H3	19	6	4	10	60	40
H4	19	8	21	29	28	72
H5	180	9	17	26	35	65
M1	15	8	14	22	36	64
M2	69	8	38	46	17	83
M3	40	12	30	42	29	71
M4	27	3	9	12	25	75
M5	21	15	31	46	33	67
T1	48	5	6	11	45	55
T2	141	9	20	29	31	69
T3	145	11	32	43	26	74
T4	121	7	24	31	23	77
T5	55	5	21	26	19	81

with the results of Gil-Duran et al. (2016). There is a comparatively higher variation in the strength as evident in Fig. 5B, especially for scales of the head and middle regions, where the coefficient of variation is greater than 0.35. While there are less pronounced variations in the elastic modulus of the scales within a region (Fig. 5A), there are significant differences across the anatomical locations.

Owing to the higher degree of mineralization of the collagen matrix of the samples H3 and M4, they would be expected to have higher strength and elastic modulus than the other scales in their respective anatomical groups. Indeed, the elastic modulus and strength of specimen H3 is the largest of that for scales of the head group (Fig. 5A) and overall. However, specimen M4 exhibited an elastic modulus and strength that was lower than the average of these properties.

The EE ratio was estimated for each of the scales using the measures of the relative layer thickness. Fig. 6 shows the distribution of elastic modulus (Fig. 6A) and strength (Fig. 6B) in terms of the EE ratio of scales from the three regions. Clearly, a larger proportion of mineralized plies in the elasmodine results in a higher elastic modulus and strength. These trends agree with the recent findings of previous studies reported on carp scales (Murcia et al., 2016a, 2016b). Nevertheless, to understand the role of each layer on the mechanical behavior, further exploration is necessary.

In previous evaluations of fish scales, the strength of the IE has been demonstrated to be higher than the strength of the whole scale when it includes the EE and LL layers (Zhu et al., 2012; Gil-Duran et al., 2016), as summarized in Table 1. Mineralization of the collagen matrix reduces the propensity for plastic strain (Maciel et al., 1996; Pashley et al., 2003; Murcia et al., 2016b). As a consequence, the strength of the scales is limited by the strain to failure of the mineralized layers (EE) and would be expected to depend on the EE ratio, as well as the relative mineral content of the EE. Indeed, there is a strong correlation between the experimental strain to failure (ε^*) and the EE ratio as shown in Fig. 7 for the tarpon scales. That dependence can be defined in terms of a linear relationship according to

$$\varepsilon^* = k_1 * EE_{ratio} - k_2 \quad (14)$$

where k_1 and k_2 are constants determined experimentally that are dependent on fish species and level of mineralization. A best fit of the experimental results from Fig. 7 for the tarpon scales result in k_1 as 0.384 and k_2 as −0.019.

In previous studies, the tensile strength of fish scales has been defined as the maximum stress recorded just prior to the first significant drop in stress (Garrano et al., 2012). Stress vs strain curves for selected tarpon scales obtained from the three regions of evaluation are shown to the first major load drop in Fig. 8A. For scales of the head and middle regions, the curve can be divided into two zones as shown in Fig. 8B. The initial portion of the curve is linear and defines the elastic response, which quantifies the elastic modulus of the composite (E^*). The response is linear, until failure of the LL, which was identified by the change in slope. Although this behavior was common for scales from all the regions, it was most distinct for scales of the head and middle regions. In addition, the strain at failure of the LL varied between regions. Failure of the LL occurred at a strain of roughly 0.04 ± 0.01 for scales of the head and middle regions, as indicated by the dotted line in Fig. 8B. After this point, the scales exhibited a second linear regime that reflects

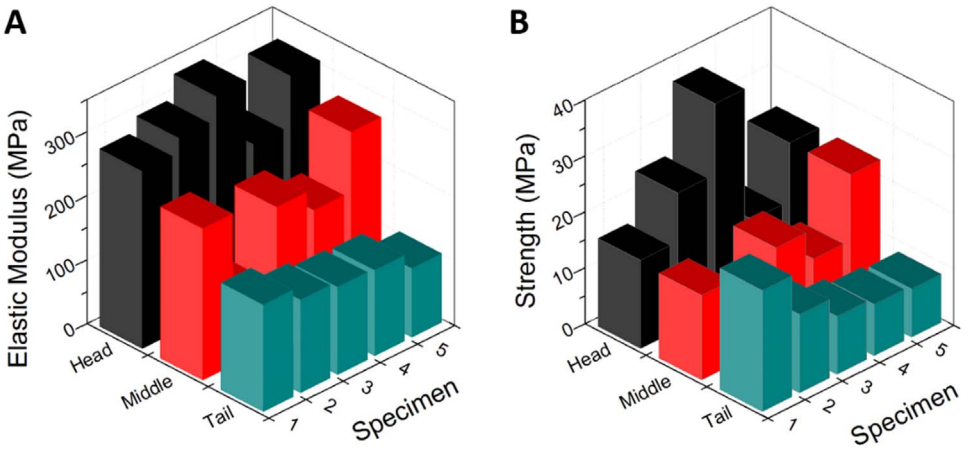

Fig. 5. Mechanical properties of tarpon scales from the head, middle and tail regions. (A) Elastic modulus; (B) Strength. The strength is defined as the stress at first axial ply failure of the elasmodine.

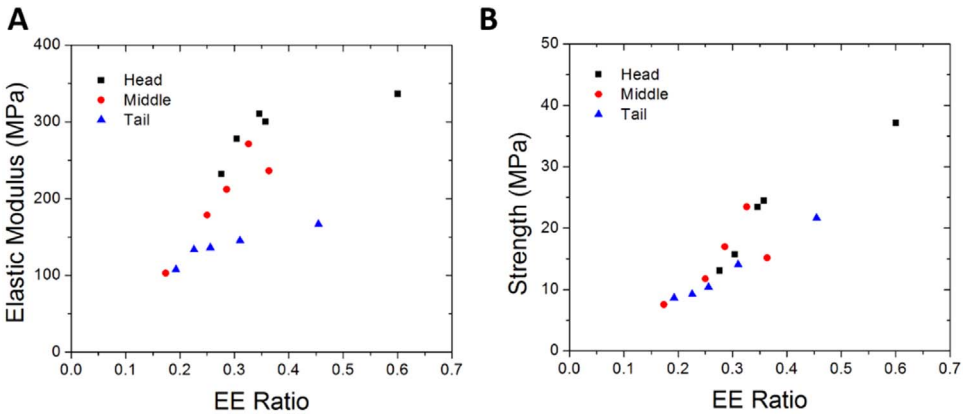

Fig. 6. Mechanical properties of the tarpon scales from the three regions plotted in terms of the external elasmodine (EE) ratio: (A) elastic modulus, (B) strength.

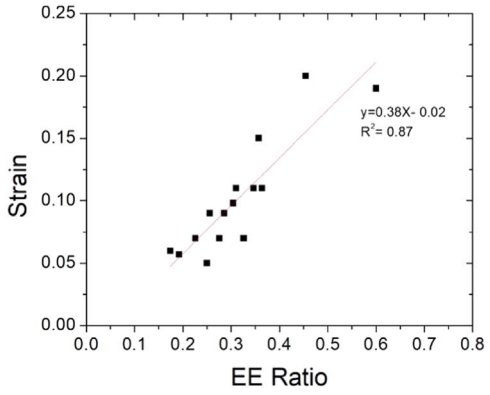

Fig. 7. Correlation between the strain to failure and the EE ratio for scales from the three regions of the tarpon.

the elastic modulus of the elasmodine (E′), including contributions from both the EE and IE. This second regime of linear behavior ends at the first major load drop, which corresponds to the first axial ply failure of the elasmodine. Using this event to define "failure", the strength of scales from the head and middle regions can be simply modeled as:

$$S = cE^* + \varepsilon^* E' \quad (15)$$

where c represents a constant defined at the strain to failure of the LL. For the tarpon, this value is equal to 0.42, but it is expected that this value may vary according to fish species and age. The value ε* represents the predicted strain at first ply failure according to the EE ratio and relationship defined by Eq. (14). For scales of the tail, changes in the integrity of the LL with strain were not evident, and failure was defined at the first load drop, as evident in Fig. 8A. Therefore, the strength for tail scales can be estimated by multiplying the predicted strain to failure (ε^*) by the elastic modulus of scales from this area.

4. Discussion

Over the past decade, a number of evaluations have been performed on the structural behavior of fish scales. The results reported in these studies have established the potential for scales to serve as a model in the design of new multi-functional engineering materials. Surprisingly though, very few of these studies have explored the properties of scales over the anatomical regions of the fish (Garrano et al., 2012; Murcia et al., 2015; Gil-Duran et al., 2016). As evident from results describing the elastic modulus and strength in Fig. 5, there are distinct differences in scale properties across the body of the tarpon. Possible explanations include selective reinforcement to protect areas with vital organs (Garrano et al., 2012), the differences in time from scale eruption to maturity that has regulated the degree of mineralization achieved (Murcia et al., 2016a), or simply Nature's response to the location-specific multi-functional requirements. All of these reasons are plausible. In the present work, a semi-empirical model is presented for predicting the elastic properties of fish scales and to further understand the relationship between scale structure and properties.

The thickness of the LL is significantly lower than that of the EE and IE, regardless of the anatomical location (Fig. 4). Nevertheless, it is the most highly mineralized layer and possesses an elastic modulus that is several orders of magnitude higher than that of the IE. While the EE is also highly mineralized, its overall contribution to the in-plane scale stiffness is limited by the misalignment of the plies (Fig. 3). The mineral content of the individual layers of the scales is not significantly different between anatomical locations in fish of the same species (Murcia et al., 2016b). As such, the significant differences in E* of the scales between anatomical regions (Fig. 5A) is expected to be primarily attributed to the variations in LL thickness. Nevertheless, the spatial variations in the elastic modulus in Fig. 5A could also be related to specific qualities of the mineral crystals.

Mineralization of fish scales is driven by a cellular process and there is evidence suggesting that the aspect ratio of the apatite crystals among

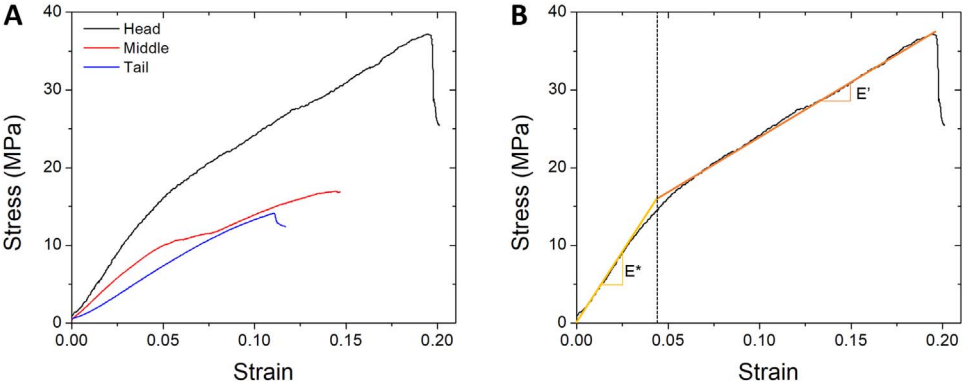

Fig. 8. Stress vs strain responses for the tarpon scales. (A) Representative head, middle and tail scales of the tarpon. The initial response of head and middle scales was divided into two regions as shown in (B). An elastic modulus of the scales was defined (E*) according to the initial linear region. After failure of the limiting layer, the response transitions into a second region defined by the elastic response of the elasmodine (E′). On average, the transition from E* to E′ occurred at a strain of 0.041 ± 0.01 m/m for the head and middle scales. Contrary to the head and middle regions, scales from the tail showed the first significant change in slope after failure of the elasmodine as shown in (A).

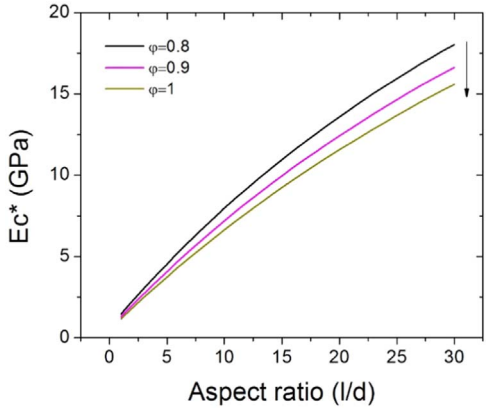

Fig. 9. Effect of the mineral crystal aspect ratio (l/d) and the packing factor (ϕ) on the elastic modulus of limiting layer.

species is different (Schönbörner et al., 1979; Zylerberg, 1985; Murcia et al., 2016a). Under that condition, the scale stiffness is not simply a function of the LL thickness. For instance, the aspect ratio and packing fraction of the mineral crystals are important to consider in estimating the elastic modulus of the LL. In previous studies of bone and dentine, an aspect ratio between 25 and 30 was selected (Currey, 1969; Nair et al., 2013). Deproteinization of *Arapaima gigas* scales revealed a randomly oriented mineral phase with a platelet morphology. The plates showed average dimensions of 50 nm thickness and 500 nm diameter (Lin et al., 2011), which results in an aspect ratio of 10. The packing fraction of the reinforcement has been suggested to have a maximum value of 0.82 for random fibers. The importance of crystal aspect ratio and its packing fraction to the elastic modulus of the LL is shown in Fig. 9. Values of packing fraction higher than 0.82 result in a decrease of the elastic modulus of the LL. Clearly, variations in the aspect ratio have greater influence on the elastic modulus than the packing fraction. To the authors' knowledge, a comparison of the apatite crystal dimensions among fish species and its influence on scale stiffness and other components of the structural behavior has not been reported. This is an interesting consideration and extends the possibilities for bioinspiration. There may also be spatial variations in the crystal aspect ratio, which would enable further modulation of scale stiffness over the body of the fish.

Using the models for each layer, an estimate for the individual layer contributions to the overall elastic modulus of scales from the three regions is shown in Fig. 10A. Contrary to earlier interpretations (Murcia et al., 2015), the elastic modulus of the scales is heavily dependent on the LL, and is most important to scales of the head region. Contribution of the EE is limited due to its lower total volume fraction than the IE across anatomical regions. The EE could have a greater contribution if more plies of the elasmodine are aligned with the loading axis, which is relevant for specific species. A comparison of the predicted elastic modulus of the scales with the experimental results is presented in Fig. 10B in terms of the volume fraction of the LL. For best agreement between the predicted and experimental responses, the average aspect ratio of the mineral crystals in the head, middle and tail scales were 3.0, 2.4 and 1.0, respectively. Excluding the response of specimen M4, which failed prematurely and resulted in a difference > 100%, the maximum "error" between the prediction and experimental result is 25%; the average difference is 7%. This range lies well within the extent of natural variation in mechanical properties of the scales within a specific region (Lin et al., 2011; Garrano et al., 2012; Zhu et al., 2012; Murcia et al., 2015, 2016b; Gil-Duran et al., 2016).

To this point, all of the spatial variations in scale properties have been interpreted to be related to the mineral content. Another potential contribution to differences in the elastic modulus across regions could result from cross-linking of the collagen in both the IE and EE. Cross-

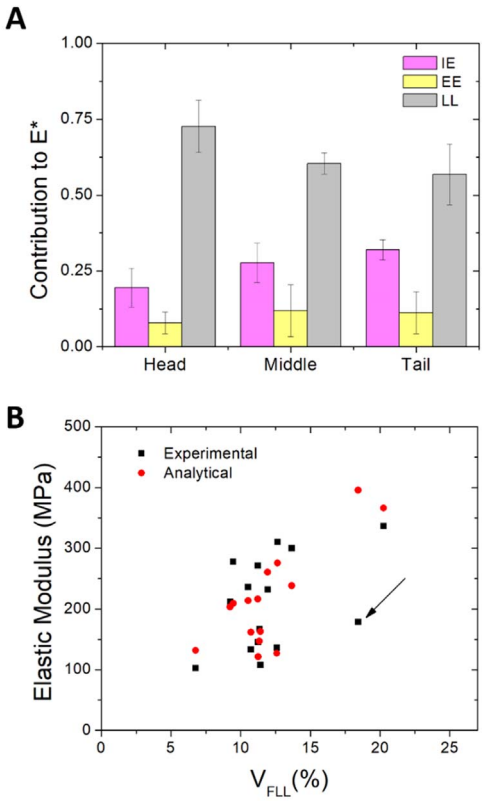

Fig. 10. Elastic modulus of the scales and predictions from the proposed model. (A) Average contribution of the LL, EE and IE to the elastic modulus of the scales within the three regions. (B) Comparison of the experimental and predicted values and their dependence on the volume fraction of the LL ($V_{f,LL}$). The arrow highlights specimen M4, which failed prematurely and resulted in a difference between experiment and prediction of over 100%.

linking has been shown to have an effect on the mechanics of collagen (Depalle et al., 2015) and could be an important factor to the structural behavior of scales, especially considering the volume fraction of the IE (Fig. 2). An increase in cross-linking would resist sliding and stretching of the tropocollagen molecules, thereby increasing both the stiffness and strength of the collagen, as well as of the scales overall. While plausible, the cause of the cross-linking and sources for spatial variations comes to question. That could occur with maturation of the scales with age as it does in other hard tissues, or result from differences in the mineral content and available sites for cross-linking. Clearly this is speculation and requires further study.

The constitutive behavior of the scales was described using a simple bi-linear model as shown in Fig. 8B. The initial linear regime defines the elastic modulus of the tri-layer composite, which was modeled as a material system of springs in parallel. The initial linear response is largely dictated by the elastic moduli of the more highly mineralized layers, i.e. the LL and EE. In response to the axial deformation the LL fails first due to the high mineral content and transfers its load share to the elasmodine. According to the tensile response in Fig. 8, failure of the LL occurs at approximately 4% strain, and the elasmodine continues to undergo linear inelastic deformation thereafter until first ply failure of axial plies of the EE. A comparison of the predicted strength of the tarpon scales (Eq. (15)) with the experimental results is shown in Fig. 11 for the three anatomical regions. The predicted tensile strength of head and middle scales (Fig. 11A and B, respectively) was within an average error of 16%. Meanwhile, the predicted strength of the tail scales (Fig. 11C) was predicted with an average error of 2%.

Similar to the comparison of experimental and predicted elastic moduli, the predicted strength of specimen M4 did not agree with the experimental measurement (difference > 150%). Previous studies

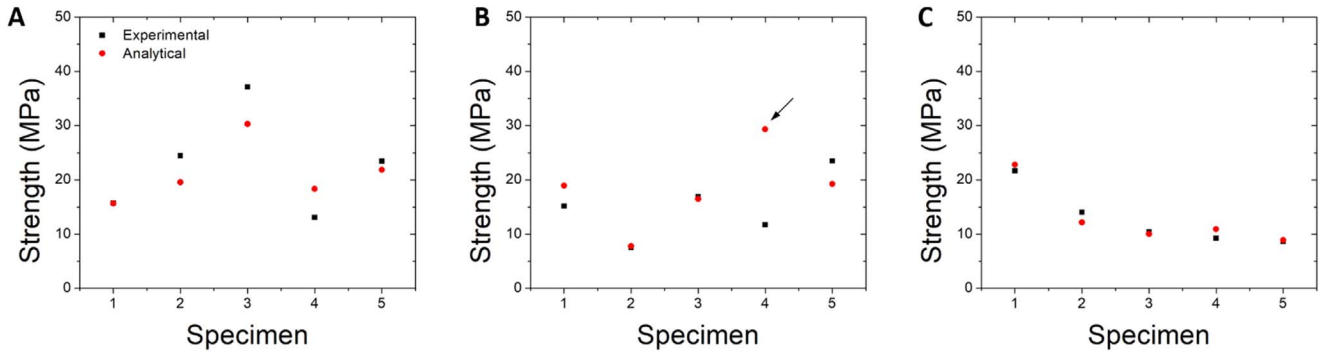

Fig. 11. Prediction of the strength of the tarpon scales from the three regions. (A) head, (B) middle, (C) tail. Note the arrow in (B), which highlights specimen M4. This scale failed prematurely resulting in a prediction error of over 100%.

performed on tarpon scales reported large variations in strength, even within anatomical regions (Gil-Duran et al., 2016). Although some variation is undoubtedly a consequence of the unique layer distribution through the thickness of the scales (Fig. 4), a more likely contribution is that the scale possessed defects in the EE that resulted in significantly lower elastic modulus and strength. Liu et al. (Liu et al., 2017) recently characterized tensile failure of scales as a three step process that involves fracture of the LL, followed by an increase in deformation until delamination of the mineralized layers from the IE. Premature failure of the LL and EE initiating from defects can cause variations in the elastic modulus and strength. The surface of the LL is populated by the presence of circuli and radii, which are important to the scale flexibility (Zhu et al., 2012; Gil-Duran et al., 2016; Murcia et al., 2017). The radii extend within the elasmodine and are the most likely contribution to premature failure of the scales under an axial loading configuration. Of course, the introduction of defects during the stamping process of the tensile specimens could facilitate premature failure and early transition from the first to the second region of deformation defined in Fig. 8B. It is important to highlight that the predicted strength of the tail scales agreed very well with the experimental results (Fig. 11C). The tail scales did not appear to be influenced by defects, as expected, due to the lower number of mineralized plies.

Results from this study have provided quantitative descriptions for the relative contributions of the layered structure to the mechanical behavior of elasmoid fish scales. The structural behavior of the scales was shown to depend on contributions from the microstructural features of each layer and that there are spatial variations in the relative contributions of the layers. Although the EE ratio is important to the elastic modulus and strength of scales (Fig. 6), the primary contribution to these properties comes from the LL (Fig. 10A). In scales of the tarpon, up to nearly 75% of the initial scale stiffness is attributed to the LL, and the largest contribution of this layer is in scales of the head region. Due to misalignment of the minerals with respect to the loading direction, an increase in the mineralization of the elasmodine has less influence on the tensile response overall.

Although the results provide additional understanding of fish scales as a structural material, there are some concerns and limitations that are necessary to address. The strength of the scales was defined in terms of the first axial ply failure of the external elasmodine. That definition is appropriate for engineering applications, but may not be the most appropriate for the multi-functional performance required by the fish. Additional consideration of the definitions used for the strength of fish scales is recommended, especially if a comparison between species will be performed. Furthermore, as a result of the analytical modeling it was found that the scale properties potentially depend on other aspects of the scale microstructure, which have not been explored in detail experimentally. For instance, there is evidence that the aspect ratio of mineral crystals of the LL contribute to its elastic modulus, which is critical to the scales overall. Consequently, future work concerning the mineral crystals of the LL is warranted. In addition, collagen crosslinking was not considered in the modeling, but could contribute substantially to the elastic modulus and strength, especially near the tail where the mineralized content plays a lesser role. These details are at the heart of the materials science of fish scales, and are ripe topics to be explored in future work.

5. Conclusions

A semi-empirical model was developed to quantify the elastic behavior of elasmoid fish scales in terms of the relative contribution of the three primary layers, including the limiting layer (LL) and the external (EE) and internal elasmodine (IE). Due to the limited information for the elastic modulus of the EE and LL, estimates were obtained from a rule of mixtures approach that accounts for the geometry of the mineral reinforcement. The findings show that although the elastic modulus of individual plies of the EE can be orders of magnitude higher than that of non-mineralized collagen, the ply rotations of the twisted plywood structure result in a significantly lower elastic modulus of the scale, and hence lower stiffness overall. The LL plays the largest role on the elastic response, followed by the internal elasmodine (IE), which has a significant contribution that varies with anatomical location. Results for predictions of the elastic modulus were within 7% average error with experimental results for tarpon scales, and well within the variation in properties of natural fish scales. Experimental variations of strength across scales within a single anatomical region were found to be potentially related to brittle failure due to the presence of defects in the LL and EE.

References

An, K.-N., Sun, Y.-L., Luo, Z.-P., 2004. Flexibility of type I collagen and mechanical property of connective tissue. Biorheology 41, 239–246.
Bigi, A., Burghammer, M., Falconi, R., Koch, M.H., Panzavolta, S., Riekel, C., 2001. Twisted plywood pattern of collagen fibrils in teleost scales: an X-ray diffraction investigation. J. Struct. Biol. 136, 137–143.
Bouslama, N., Chevalier, Y., Bouaziz, J., Ayed, F.B., 2013. Influence of the sintering temperature on Young's modulus and the shear modulus of tricalcium phosphate–-fluorapatite composites evaluated by ultrasound techniques. Mater. Chem. Phys. 141, 289–297.
Bruet, B.J., Song, J., Boyce, M.C., Ortiz, C., 2008. Materials design principles of ancient fish armour. Nat. Mater. 7, 748–756.
Chintapalli, R.K., Mirkhalaf, M., Dastjerdi, A.K., Barthelat, F., 2014. Fabrication, testing and modeling of a new flexible armor inspired from natural fish scales and osteoderms. Bioinspir. Biomim. 9, 036005.
Currey, J.D., 1969. The relationship between the stiffness and the mineral content of bone. J. Biomech. 2, 477–480.
Depalle, B., Qin, Z., Shefelbine, S.J., Buehler, M.J., 2015. Influence of cross-link structure, density and mechanical properties in the mesoscale deformation mechanisms of collagen fibrils. J. Mech. Behav. Biomed. Mater. 52, 1–13.
Funk, N., Vera, M., Szewciw, L.J., Barthelat, F., Stoykovich, M.P., Vernerey, F.J., 2015. Bioinspired fabrication and characterization of a synthetic fish skin for the protection of soft materials. ACS Appl. Mater. Interfaces 7, 5972–5983.
Garrano, A.M.C., La Rosa, G., Zhang, D., Niu, L.-N., Tay, F., Majd, H., Arola, D., 2012. On the mechanical behavior of scales from Cyprinus carpio. J. Mech. Behav. Biomed. Mater. 7, 17–29.

Gil-Duran, S., Arola, D., Ossa, E., 2016. Effect of chemical composition and microstructure on the mechanical behavior of fish scales from Megalops atlanticus. J. Mech. Behav. Biomed. Mater. 56, 134–145.
Hench, L.L., Wilson, J., 1993. An Introduction to Bioceramics. World scientific.
Jandt, K.D., 2008. Biological materials: fishing for compliance. Nat. Mater. 7, 692–693.
Jones, R.M., 1998. Mechanics of Composite Materials. CRC Press.
Kato, Y.P., Christiansen, D.L., Hahn, R.A., Shieh, S.-J., Goldstein, J.D., Silver, F.H., 1989. Mechanical properties of collagen fibres: a comparison of reconstituted and rat tail tendon fibres. Biomaterials 10, 38–42.
Li, Y., Ortiz, C., Boyce, M.C., 2012. Bioinspired, mechanical, deterministic fractal model for hierarchical suture joints. Phys. Rev. E 85, 031901.
Lin, Y., Wei, C., Olevsky, E., Meyers, M.A., 2011. Mechanical properties and the laminate structure of Arapaima gigas scales. J. Mech. Behav. Biomed. Mater. 4, 1145–1156.
Liu, P., Zhu, D., Wang, J., Bui, T.Q., 2017. Structure, mechanical behavior and puncture resistance of grass carp scales. J. Bionic Eng. 14, 356–368.
Lu, Y., 2002. Mechanical properties of random discontinuous fiber composites manufactured from wetlay process.
Maciel, K., Carvalho, R., Ringle, R., Preston, C., Russell, C., Pashley, D.H., 1996. The effects of acetone, ethanol, HEMA, and air on the stiffness of human decalcified dentin matrix. J. Dent. Res. 75, 1851–1858.
Martini, R., Barthelat, F., 2016. Stability of hard plates on soft substrates and application to the design of bioinspired segmented armor. J. Mech. Phys. Solids 92, 195–209.
McNally, E.A., Schwarcz, H.P., Botton, G.A., Arsenault, A.L., 2012. A model for the ultrastructure of bone based on electron microscopy of ion-milled sections. Plos ONE 7 (1), e29258.
Murcia, S., Lavoie, E., Linley, T., Devaraj, A., Ossa, E.A., Arola, D., 2016a. The natural armors of fish: a comparison of the lamination pattern and structure of scales. J. Mech. Behav. Biomed. Mater.
Murcia, S., Li, G., Yahyazadehfar, M., Sasser, M., Ossa, A., Arola, D., 2016b. Effects of polar solvents on the mechanical behavior of fish scales. Mater. Sci. Eng.: C 61, 23–31.
Murcia, S., McConville, M., Li, G., Ossa, A., Arola, D., 2015. Temperature effects on the fracture resistance of scales from Cyprinus carpio. Acta Biomater. 14, 154–163.
Murcia, S., Stossel, M., Pahuja, R., Linley, T., Devaraj, A., Ramulu, M., Ossa, E., Wang, J., Arola, D., 2017. The limiting layer of fish scales: structure and properties. Acta Biomater (submitted for publication).
Nair, A.K., Gautieri, A., Chang, S.-W., Buehler, M.J., 2013. Molecular mechanics of mineralized collagen fibrils in bone. Nat. Commun. 4, 1724.
Nielsen, L., Chen, P., 1968. Young's modulus of composites filled with randomly oriented fibers. J. Mater.
Nielson, L.E., 1974. Mechanical Properties of Polymer and Composites. Marcel Dekker.
Pashley, D.H., Agee, K.A., Carvalho, R.M., Lee, K.-W., Tay, F.R., Callison, T.E., 2003. Effects of water and water-free polar solvents on the tensile properties of demineralized dentin. Dent. Mater. 19, 347–352.
Pins, G.D., Silver, F.H., 1995. A self-assembled collagen scaffold suitable for use in soft and hard tissue replacement. Mater. Sci. Eng.: C 3, 101–107.
Schönbörner, A., Boivin, G., Baud, C., 1979. The mineralization processes in teleost fish scales. Cell Tissue Res. 202, 203–212.
Schwarcz, H.P., McNally, E.A., Botton, G.A., 2014. Dark-field transmission electron microscopy of cortical bone reveals details of extrafibrillar crystals. J. Struct. Biol. 188, 240–248.
Sherman, V.R., Quan, H., Yang, W., Ritchie, R.O., Meyers, M.A., 2016. A comparative study of piscine defense: the scales of Arapaima gigas, Latimeria chalumnae and Atractosteus spatula. J. Mech. Behav. Biomed. Mater.
Sire, J.-Y., Huysseune, A., 2003. Formation of dermal skeletal and dental tissues in fish: a comparative and evolutionary approach. Biol. Rev. 78, 219–249.
Sire, J.-Y., Quilhac, A., Bourguignon, J., Allizard, F., 1997. Evidence for participation of the epidermis in the deposition of superficial layer of scales in zebrafish (Danio rerio): a SEM and TEM study. J. Morphol. 231, 161–174.
Yang, L., Werf, K.O., Van der, Fitié, C.F., Bennink, M.L., Dijkstra, P.J., Feijen, J., 2008. Mechanical properties of native and cross-linked type I collagen fibrils. Biophys. J. 94, 2204–2211.
Yang, W., Chen, I.H., Gludovatz, B., Zimmermann, E.A., Ritchie, R.O., Meyers, M.A., 2013. Natural flexible dermal armor. Adv. Mater. 25, 31–48.
Yang, W., Sherman, V.R., Gludovatz, B., Mackey, M., Zimmermann, E.A., Chang, E.H., Schaible, E., Qin, Z., Buehler, M.J., Ritchie, R.O., et al., 2014. Protective role of Arapaima gigas fish scales: structure and mechanical behavior. Acta Biomater. 10, 3599–3614.
Zhang, D., Nazari, A., Soappman, M., Bajaj, D., Arola, D., 2007. Methods for examining the fatigue and fracture behavior of hard tissues. Exp. Mech. 47, 325–336.
Zhu, D., Ortega, C.F., Motamedi, R., Szewciw, L., Vernerey, F., Barthelat, F., 2012. Structure and mechanical performance of a “modern’ fish scale. Adv. Eng. Mater. 14, B185–B194.
Zhu, D., Szewciw, L., Vernerey, F., Barthelat, F., 2013. Puncture resistance of the scaled skin from striped bass: collective mechanisms and inspiration for new flexible armor designs. J. Mech. Behav. Biomed. Mater. 24, 30–40.
Zimmermann, E.A., Gludovatz, B., Schaible, E., Dave, N.K., Yang, W., Meyers, M.A., Ritchie, R.O., 2013. Mechanical adaptability of the Bouligand-type structure in natural dermal armour. Nat. Commun. 4, 2634.
Zylberberg, D.L., Nicolas, G., 1982. Ultrastructure of scales in a teleost (Carassius auratus L.) after use of rapid freeze-fixation and freeze-substitution. Cell Tissue Res. 223, 349–367.
Zylerberg, L., 1985a. Collagen and Mineralization in the Elasmoid Scales, Biology Intervertebrate Lower Vertebrate Collagens. Springer, pp. 457–463.